Supplementary Information for
"Observation of plaquette fluctuations in the spin-1/2 honeycomb lattice"

Christian Wessler[1]*, Bertrand Roessli[1], Karl W. Krämer[2], Bernard Delley[1], Oliver Waldmann[3], Lukas Keller[1], Denis Cheptiakov[1], Hans B. Braun[4,5] & Michel Kenzelmann[1]

[1]Laboratory for Neutron Scattering and Imaging, Paul Scherrer Institut, Villigen, Switzerland
[2]Department of Chemistry and Biochemistry, University of Bern, Bern, Switzerland
[3]Physikalisches Institut, Universität Freiburg, Freiburg, Germany
[4]Theoretical Physics, ETH Zürich, Switzerland
[5]Dublin Institute for Advanced Studies, Dublin 4, Ireland
*To whom correspondence should be addressed; E-mail: christian.wessler@psi.ch

1

Supplementary Note 1. CRYSTAL STRUCTURE

$YbBr_3$ crystallizes with the BiI_3 layer structure in the rhombohedral space group $R\bar{3}$ (148) with lattices parameters of $a = 6.97179(18)$ Å and $c = 19.1037(7)$ Å at room temperature. The lattice parameters are in good agreement with powder[1] and crystal[2] diffraction data found in literature. The unit cell contains six Yb^{3+} ions on site (6c) at (0, 0, z), (0, 0, z) + (2/3, 1/3, 1/3) and (0, 0, z) + (1/3, 2/3, 2/3) with z = 0.1670(2). The Yb ions have C_3 point symmetry and form two-dimensional (2D) honeycomb lattices perpendicular to the c-axis, see Fig. 1. Yb^{3+} has a distorted octahedral coordination by Br^- ions which are located on site (18f) at (x, y, z) with x=0.3331(5), y=0.3131(5), and z=0.08336(15). Surprisingly, the distance between Yb^{3+}-Br^- varies by less than 10^{-2} Å, however the Br^--Yb^{3+}-Br^- bond angles differ significantly between 87.3° and 91.1°. The crystallographic parameters determined on HRPT are summarized in Supplementary Table 1.

Name	x	y	z	occ.
Yb1	0	0	0.33289(21)	0.317(3)
Yb2	0	0	0	0.009(0)
Br	0.35362(57)	0.00022(60)	0.08325(15)	1

Supplementary Table 1: Structural parameters of $YbBr_3$ determined on HRPT at room temperature
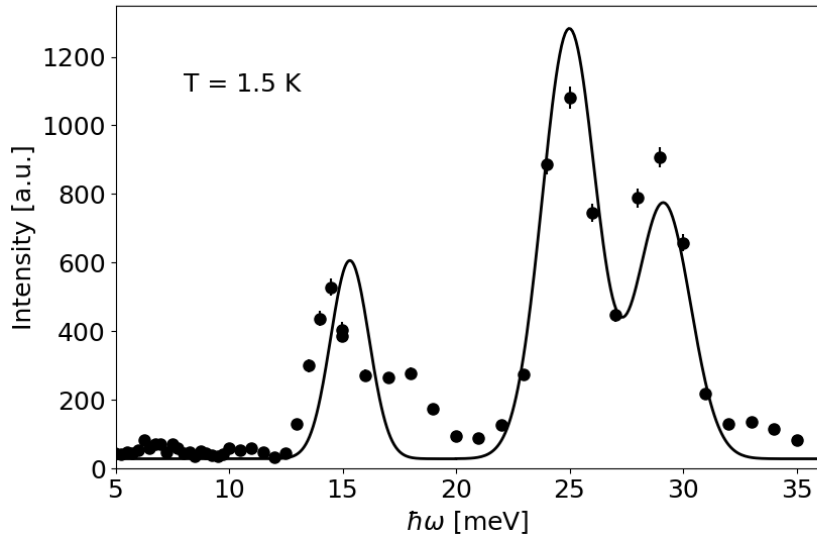
Supplementary Note 2. CRYSTAL ELECTRIC FIELD (CEF)

The electrostatic potential originating from the ions surrounding the Yb^{3+} ion can be modeled with Stevens operators

$$H_{CEF} = \sum_{l,m} B_l^m O_l^m$$

with $B_l^m = \gamma_l^m \theta_l$ and θ_l the Stevens coefficients. For the C_3 point group symmetry of the Yb site only the parameters[3] $B_2^0, B_4^0, B_4^{\pm 3}, B_6^0, B_6^{\pm 3}, B_6^{\pm 6}$ are non-zero. From the inelastic neutron scattering measurement we determined 3 CEF excitations at $E_1 = 14.5$ meV, $E_2 = 25$ meV and $E_3 = 29$ meV. We first used the susceptibility $\chi(T)$ for the determination of the CEF Hamiltonian. From a least-square fit to χ_a and χ_c where a and c denote the crystallographic axis we obtain $\gamma_2^0 = $ -5.14 meV, $\gamma_4^0 = $ -0.59 meV, $\gamma_4^{+3} = 57.43$ meV, $\gamma_4^{-3} = 51.31$ meV, $\gamma_6^0 = 6.09$ meV, $\gamma_6^{+3} = 50.21$ meV, $\gamma_6^{-3} = 55.56$ meV, $\gamma_6^{+6} = 33.9$ meV, $\gamma_6^{-6} = 42.4$ meV. In agreement with the Kramers theorem the CEF splits the $J = 7/2$ multiplet of the Yb^{3+} ion into 4 doublets. The calculated CEF-levels are at 15.16 meV, 24.75 meV, and 28.88 meV, respectively. From a subsequent fit of the inelastic neutron data we obtain very similar values, $\gamma_2^0 = $-6.49 meV, $\gamma_4^0 = $ -0.51 meV, $\gamma_4^{+3} = $58.53 meV, $\gamma_4^{-3} = $52.12 meV, $\gamma_6^0 = 6.01$ meV, $\gamma_6^{+3} = 48.11$ meV, $\gamma_6^{-3} = 56.30$ meV, $\gamma_6^{+6} = 33.21$ meV, $\gamma_6^{-6} = 41.12$ meV. We show in Supplementary Fig. 1 a comparison between calculated and observed neutron scattering intensities. We point out that the first excited CEF-level has a double-peak structure in $YbBr_3$ that is not explained by our model. It also resembles the CEF levels[4] of $YbCl_3$ and

thus this issue requires further investigation. Nevertheless the CEF-model presented here provides an adequate description of the temperature dependence of the static susceptibility. In addition we performed a point charge calculation based on the program multiX.[5] In agreement with the susceptibility measurements, calculations show that at high temperatures anisotropy is small in YbBr$_3$ with easy-plane anisotropy developing below $T = 50$ K. At $T = 4$ K, we obtain $\chi_a \approx 1.3\chi_c$.

Supplementary Fig. 1 | Yb^{3+} crystal electric field in YbBr$_3$. Crystal electric field (CEF) excitations measured by inelastic neutron scattering. The solid line is the calculated intensity. Error bars are standard deviations.

Supplementary Note 3. MAGNETIC EXCITATIONS

Because of the large separation between the ground-state and the first CEF doublet, the magnetic properties of YbBr$_3$ can be approximated by a spin $S = 1/2$. Choosing a local coordinate frame with the ζ-axis oriented along a given spin direction, the non-zero elements of the single-ion susceptibility matrix are $\chi_0^{\xi\xi}(\omega) = \chi_0^{\eta\eta}(\omega)$ and $\chi_0^{\xi\eta}(\omega) = -\chi_0^{\eta\xi}(\omega)$ which correspond to excitations transverse to the (local) spin direction. Within mean-field approximation,

$$\chi_0^{\xi\xi}(\omega) = \frac{1}{2}\frac{\Delta}{\Delta^2 - (\omega + i\epsilon)^2} \tag{1}$$

$$\chi_0^{\xi\eta}(\omega) = \frac{i}{2}\frac{\omega + i\epsilon}{\Delta^2 - (\omega + i\epsilon)^2}, \tag{2}$$

with $\Delta \equiv \Delta_i = -\langle S_\zeta \rangle \sum_j \mathcal{J}_{\zeta\zeta}(i,j)$ the local field acting on a given Yb moment with $\mathcal{J}$ defined in Eq. (1) and ϵ the finite line width of the excitations. Within linear spin-wave theory, the dipole-dipole interactions induce a gap in the spin-wave dispersion.[9,10] With a Yb magnetic moment of 2 μ_B, the dipolar interactions produce a spin gap at the zone center ~ 200 μeV. The easy-plane anisotropy favors alignment of the spins in the hexagonal plane. The spin gap opened by H_{dip} is reduced by the easy-plane anisotropy. At $g_{\text{crit}} \sim 0.985$ the spin gap is minimal and below that value the spins rotate into the basal plane, see Supplementary Fig. 2. The easy-plane anisotropy lifts the degeneracy of the spin wave branches at the zone center and the splitting increases with increasing anisotropy.
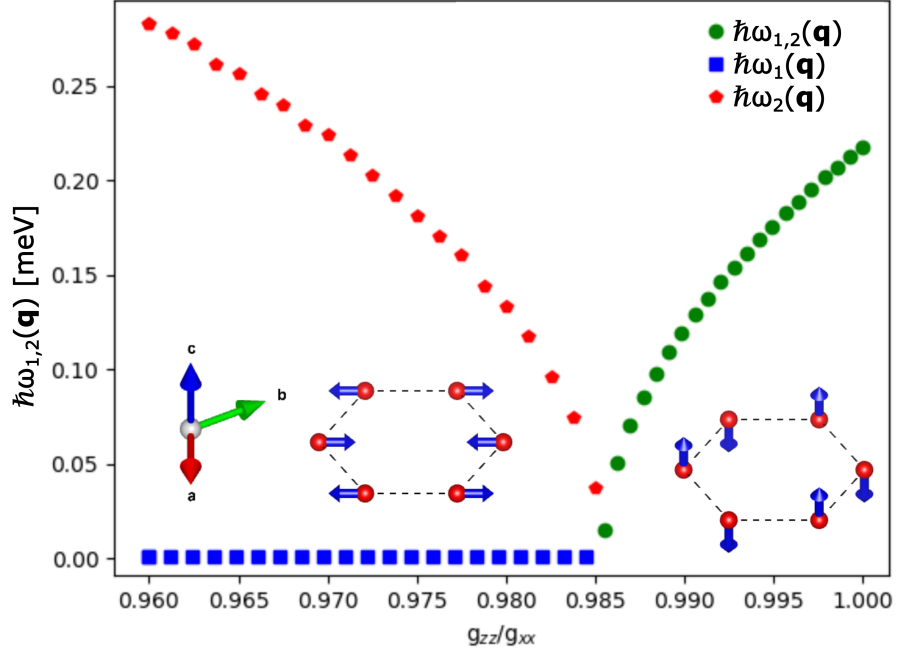
Supplementary Fig. 2 | Dependence of the energy gap as a function of easy-plane anisotropy. Above $g_{zz}/g_{xx} = 0.985 = g_{crit}$, the calculated branches $\omega_1(q)$ and $\omega_2(q)$ are degenerate while for $g_{zz}/g_{xx} < g_{crit}$ the two spin-wave branches split. All points are calculated with a precision of $\sim$ 0.005 meV. The magnetic configurations shown in the figure correspond to a Néel antiferromagnet with spins aligned along the c-axis for $g_{zz}/g_{xx} > 0.985$ and in the hexagonal plane for $g_{zz}/g_{xx} < 0.985$.

We have also simulated the two-magnon scattering expected for a Heisenberg Hamiltonian[11] as shown in Supplementary Fig. 3. for the the (1,0,0) Brlllouin zone. Our calculations show a broad continuum extending up to twice the maximum of the spin wave excitations. In contrast to our observations, the two-magnon continuum is present in the complete Brillouin zone and is strongest close to the zone center.
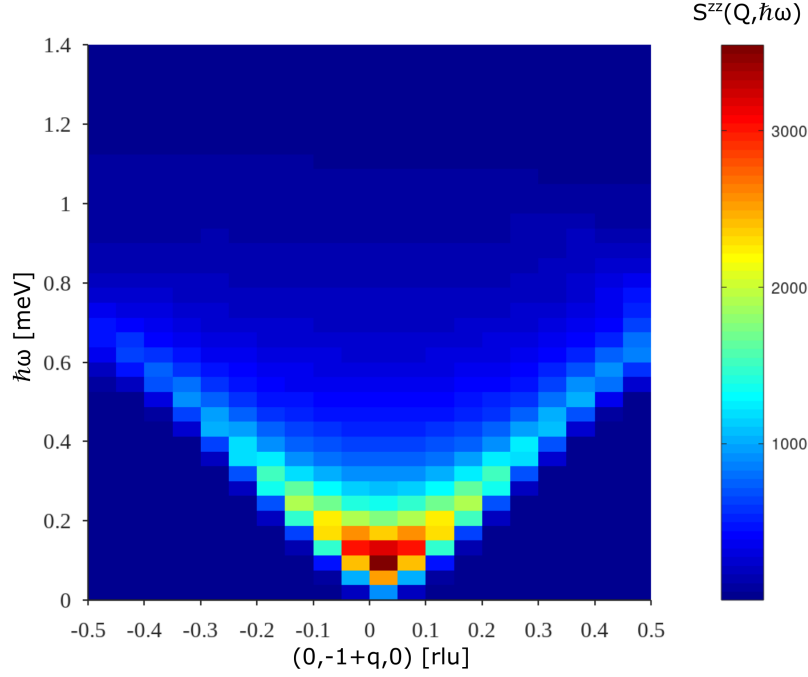
Supplementary Fig. 3 | Calculated two-magnon cross-section for a Heisenberg Hamiltonian. An arbitrary cutoff is introduced in the dispersion of the spin-waves to avoid divergence of the two-magnon cross-section at the zone center.

Supplementary Note 4. MAGNETIC GROUND-STATE

In mean field theory, the classical ground-state is given by the eigenvectors of the largest eigenvalue $\lambda\left(\mathbf{q}\right)$ of the Fourier transform of the interaction matrix $\overline{\overline{M}}(\mathbf{q})$.[6–8] Based on the Hamiltonian $H_{\mathrm{h}} + H_{\mathrm{dip}}$, $\lambda\left(\mathbf{q}\right)$ has a maximum at $\mathbf{Q}_0 = (0,0,0)$ which agrees with the diffuse scattering observed in YbBr$_3$ (see Fig. 2a). We find that the dipolar energy becomes independent of the distance between the Yb-planes for a lattice parameter $c > 12$ Å, which

shows that the 2D limit is reached in $YbBr_3$ and inter-layer interactions can be neglected.

Supplementary Note 5. MAGNETIC SUSCEPTIBILITY

The temperature dependence of the static susceptibility χ is shown in Fig. 1c for magnetic field orientations in-plane (a-axis) and out-of-plane (c-axis). χT values (not shown) increase with temperature and do not saturate up to 300 K. The values at 300 K are 2.282 and 2.687 cm^3K/mol along the a- and c-axes, respectively. The average of 2.417 cm^3K/mol is slightly below the expectation value of 2.572 cm^3K/mol for the $^2F_{7/2}$ ground-state of Yb^{3+}. At lower temperature a maximum in the χ versus T curves is observed at $T = 2.75$ K. We have calculated the temperature dependence of the static susceptibility for an Yb_6 honeycomb with the exchange parameters determined from the spin-wave analysis and easy-plane anisotropy parameters $g_a/g_c = 1.25$. We find that the susceptibility has a broad maximum around $T \simeq 4$ K and reproduces the experimental χ (T) above 5 K well, as shown in Supplementary Fig. 4.
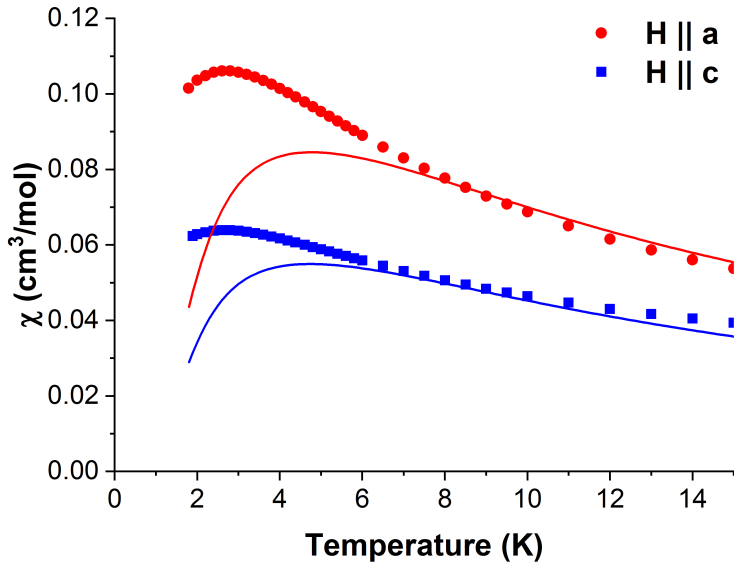
Supplementary Fig. 4 | Calculated susceptibility for a Yb$_6$ hexamer. The measured low-temperature magnetic susceptibility is shown together with the calculation (solid lines) for a single plaquette with $S = 1/2$, and the Hamiltonian $H_{\mathrm{h}} + H_{\mathrm{dip}}$ of the main text. Error bars are standard deviations.

Supplementary References

1. Meyer, G. Private communication to powder diffraction data base (PDF2), no. [42-0968] (1990).

2. Brenner, M. Kinetische Studien zu Phasenumwandlungen zwischen polymorphen Formen von $YbBr_2$ sowie die Bestimmung der Kristallstruktur von $YbBr_3$. Dissertation Universität Karlsruhe (1997).

3. Bauer, E. & Rotter, M. Magnetism of complex metallic alloys: crystalline electric field effects. in *Series on Complex Metallic Alloys* Vol. 2, ed. E. Belin-Ferr, World Scientific (2009).

4. Sala, G. *et al.* Crystal field splitting local anisotropy, and low-energy excitations in the quantum magnet $YbCl_3$. *Phys. Rev.* B **100**, 180406(R) (2019).

5. Uldry, A., Vernay, F. & Delley, B. Systematic computation of crystal-field multiplets for x-ray core spectroscopies. *Phys. Rev. B* **85**, 125133 (2012).

6. Reimers, J.N. Diffuse-magnetic-scattering calculations for frustrated antiferromagnets. *Phys. Rev. B* **46**, 193-202 (1992).

7. Kadowaki, H., Ishii, Y., Matsuhira, K. & Hinatsu, Y. Neutron scattering study of dipolar spin ice $Ho_2Sn_2O_7$: Frustrated pyrochlore magnet. *Phys. Rev. B* **65**, 144421 (2002).

8. Enjalran, M. & Gingras, M.J.P. Theory of paramagnetic scattering in highly frustrated magnets with long-range dipole-dipole interactions: The case of the $Tb_2Ti_2O_7$ pyrochlore antiferromagnet. *Phys. Rev. B* **70**, 174426 (2004).

9. Pich, C. & Schwabl, F. Order of two-dimensional isotropic dipolar anti-ferromagnets. *Phys. Rev.* B **47**, 7957-7960 (1993).

10. Pich, C. & Schwabl, F. Spin-wave dynamics of two-dimensional isotropic dipolar honeycomb antiferromagnets. *JMMM* **148**, 30-31 (1995).

11. Heilmann, I.U. *et al.* One- and two-magnon excitations in one-dimensional antiferromagnet in a magnetic field. *Phys. Rev. B* **24**, 3939-3953 (1981).